

# QUANTDEMOIRE: QUANTIZATION WITH OUTLIER AWARE FOR IMAGE DEMOIRÉING

Zheng Chen<sup>1\*</sup>, Kewei Zhang<sup>1\*</sup>, Xiaoyang Liu<sup>1</sup>, Weihang Zhang<sup>2</sup>,

Mengfan Wang<sup>2</sup>, Yifan Fu<sup>2</sup>, Yulun Zhang<sup>1†</sup>

<sup>1</sup>Shanghai Jiao Tong University, <sup>2</sup>Central Media Technology Institute, Huawei

## ABSTRACT

Demoiréing aims to remove moiré artifacts that often occur in images. While recent deep learning-based methods have achieved promising results, they typically require substantial computational resources, limiting their deployment on edge devices. Model quantization offers a compelling solution. However, directly applying existing quantization methods to demoiréing models introduces severe performance degradation. The main reasons are distribution outliers and weakened representations in smooth regions. To address these issues, we propose QuantDemoire, a post-training quantization framework tailored to demoiréing. It contains two key components. **First**, we introduce an outlier-aware quantizer to reduce errors from outliers. It uses sampling-based range estimation to reduce activation outliers, and keeps a few extreme weights in FP16 with negligible cost. **Second**, we design a frequency-aware calibration strategy. It emphasizes low- and mid-frequency components during fine-tuning, which mitigates banding artifacts caused by low-bit quantization. Extensive experiments validate that our QuantDemoire achieves large reductions in parameters and computation while maintaining quality. Meanwhile, it outperforms existing quantization methods by over **4 dB** on W4A4. Code is released at: <https://github.com/zhengchen1999/QuantDemoire>.

## 1 INTRODUCTION

Image demoiréing is a low-level vision task aimed at removing colored stripes caused by frequency aliasing between display screens and imaging sensors. These artifacts degrade the perceptual quality of captured images, and interfere with subsequent visual analysis and recognition. Due to the complex and diverse forms of moiré patterns, achieving effective demoiréing remains a highly challenging task (Sidorov & Kokaram, 2002; Liu et al., 2015; Wang et al., 2023).

In recent years, with the rapid progress of deep learning, neural networks have achieved remarkable performance in demoiréing (Cheng et al., 2019; Zheng et al., 2020; Yu et al., 2022; Xu et al., 2023; Liu et al., 2025). These models can adapt to the diversity of moiré patterns, achieving excellent performance. However, they usually involve millions of parameters and heavy computation. This makes them unsuitable for edge devices such as smartphones, drones, and portable cameras (Cheng et al., 2019; Zheng et al., 2020). These devices are also the most important application scenarios. Thus, achieving efficient demoiréing while maintaining high quality is critical for practical usage.

Model quantization (Nagel et al., 2021) offers an effective solution to this challenge. It compresses weights and activations from 32-bit floating-point to low-bit (*e.g.*, 2–8 bit) integers. This can significantly reduce storage overhead while converting costly floating-point operations into efficient integer operations. Therefore, the quantization can accelerate inference and lower power consumption, making it well-suited for resource-constrained devices and hardware accelerators. Currently, quantization is widely applied to vision tasks (Esser et al., 2019; Li et al., 2023; Qin et al., 2023).

However, in the demoiréing task, there is a lack of corresponding quantization methods. Directly applying existing quantization (Jacob et al., 2018; Li et al., 2024) results in severe performance loss. The degradation arises primarily from two factors. **First**, outliers in weights and activations expand the quantization range. This reduces the precision of most effective values and weakens the demoiréing performance. **Second**, quantization weakens representations in smooth regions. It introduces banding artifacts in mid- and low-frequency components.

\*Equal contribution.

†Corresponding author: Yulun Zhang, [yulun100@gmail.com](mailto:yulun100@gmail.com)

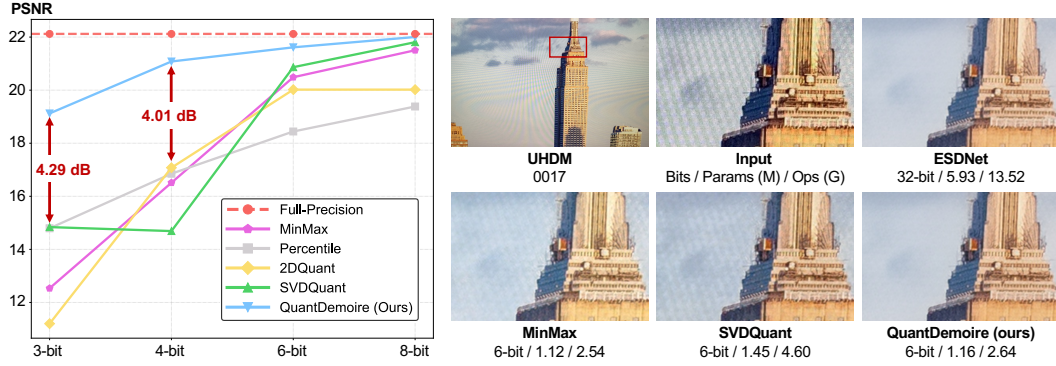


Figure 1: Comparison with recent quantization methods on UHDM (Yu et al., 2022). The full-precision backbone is ESDNet (Yu et al., 2022). Left: PSNR performance at different bit-widths. Right: visual comparison. Our QuantDemoire demonstrates superior efficiency and performance.

To address the above issues, we propose QuantDemoire, a post-training quantization (PTQ) framework tailored for image demoiréing tasks. Our core idea is to mitigate accuracy loss from two perspectives: the quantizer and the calibration. **(1) Quantizer.** We design the outlier-aware quantizer to reduce the impact of outliers. It uses random sampling to estimate and remove activation outliers. It also keeps a very small fraction of extreme weights in FP16, with negligible overhead. **(2) Calibration.** We introduce the frequency-aware calibration strategy. It explicitly emphasizes mid- and low-frequency components during the optimization of quantization parameters (*e.g.*, boundaries). This alleviates the banding in smooth regions caused by quantization.

We conduct extensive experiments to demonstrate that our QuantDemoire can achieve significant efficiency improvements while maintaining strong demoiréing performance. It consistently outperforms existing quantization methods across datasets and bit-widths. As shown in Fig. 1, compared with the full-precision model, our method reduces parameters and computation by over **86.6%** at 4-bit with less than **4.7%** (PSNR) performance drop. Besides, QuantDemoire surpasses current SOTA quantization methods by more than **4 dB** (PSNR, 4-bit) on the UHDM (Yu et al., 2022) dataset.

Our main contributions are summarized as follows:

- We propose QuantDemoire, the first quantization framework tailored to image demoiréing. It reduces model overhead while preserving strong restoration ability.
- We design the outlier-aware quantizer that mitigates quantization errors by handling outliers in both activations and weights with random sampling.
- We propose the frequency-aware calibration strategy to optimize mid- and low-frequency features, alleviating quantization-induced banding artifacts.
- We validate our method on multiple datasets and bit-widths. QuantDemoire consistently outperforms existing quantization methods quantitatively and visually.

## 2 RELATED WORK

### 2.1 IMAGE DEMOIRÉING.

When photographing content displayed on a digital screen, the captured image often exhibits colored stripes known as moiré patterns. These patterns can substantially reduce the overall quality of the image. Early approaches to moiré pattern removal primarily relied on traditional mathematical methods, such as matrix decomposition (Liu et al., 2015) and spectral models (Sidorov & Kokaram, 2002). These techniques generally perform poorly when dealing with diverse types of moiré patterns. In recent years, with the rapid development of deep learning, methods (Cheng et al., 2019; He et al., 2019; Zheng et al., 2020; He et al., 2020; Yu et al., 2022; Xu et al., 2023; Xiao et al., 2024; Liu et al., 2025), based on deep neural networks, have been proposed. MopNet (He et al., 2019) utilizes multi-scale feature aggregation and attribute-aware classifiers to handle complex frequency. To further improve performance, FHDe<sup>2</sup>Net (He et al., 2020) employs a cascaded architecture to remove multi-scale moiré patterns. Besides, ESDNet (Yu et al., 2022) integrates a semantic-aligned, scale-aware module that further improves robustness to moiré pattern scale variations. Despite favorable moiré pattern removal, these methods involve millions of parameters. The heavy computational cost makes them unsuitable for deployment on edge devices.

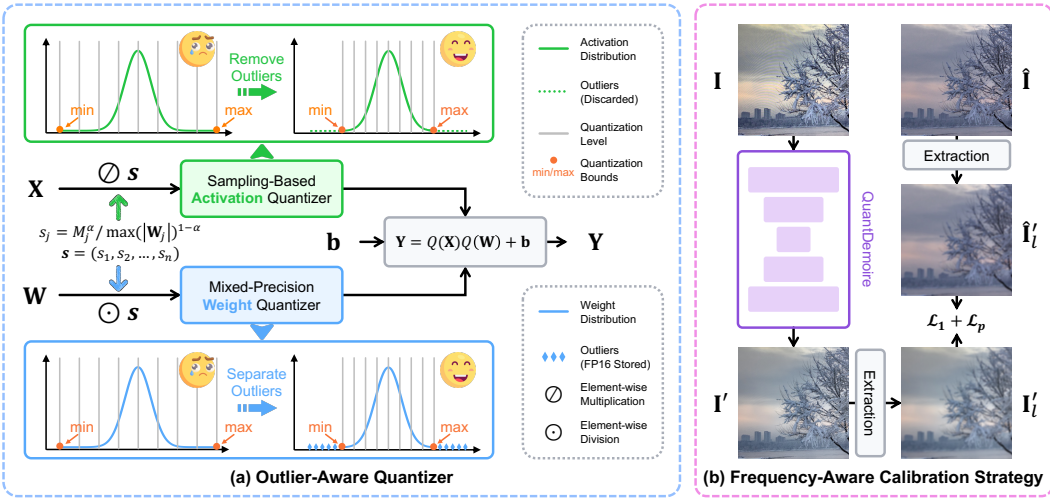


Figure 2: The overview of our QuantDemoire. (a) Outlier-Aware Quantizer: activations discard outliers through sample-based estimation, while weights preserve outliers in FP16 precision. (b) Frequency-Aware Calibration Strategy: quantizer parameters are optimized on mid- and low-frequency components, which are extracted through the frequency extraction process.

## 2.2 MODEL QUANTIZATION.

Quantization is widely used in neural network compression. By transforming weights and activations from 32-bit floating-point to low-bit integer formats, it effectively reduces both memory consumption and computational overhead. Existing quantization algorithms are generally categorized into quantization-aware training (QAT) (Esser et al., 2019; Chen et al., 2024; Qin et al., 2023) and post-training quantization (PTQ) (Liu et al., 2021; Hubara et al., 2021; Shang et al., 2023). LSQ (Esser et al., 2019) uses a learned step size to improve the performance of low-bit quantization. Although QAT achieves competitive performance (Nagel et al., 2021), its high training cost makes it less suitable for deployment on edge devices. In contrast, it is regarded as a lightweight and efficient approach, as it requires neither retraining nor labeled data. The MinMax strategy (Jacob et al., 2018) estimates quantization parameters directly from the global extrema of data distributions. SmoothQuant (Xiao et al., 2023) alleviates this issue by redistributing the quantization difficulty from activations to weights, thereby reducing activation outliers. SVDQuant (Li et al., 2024) applies singular value decomposition (SVD) to decompose the weight tensor into a low-rank component and a residual term, jointly capturing and mitigating outlier effects during quantization. Nevertheless, existing quantization methods suffer from severe performance degradation on demoiréing models. Specifically, due to the influence of outliers (Dettmers et al., 2022) and the reduced information density caused by quantization, the output image quality of quantized models deteriorates significantly, manifesting as color banding and poor moiré removal performance.

## 3 METHOD

In this section, we present our quantization framework, QuantDemoire, for efficient demoiréing (see Fig. 2). We elaborate on two key components. The first is the outlier-aware quantizer, which reduces the quantization error introduced by outliers in activations and weights. The second is the frequency-aware calibration strategy, which selectively emphasizes low- and mid-frequency components to mitigate the tone banding in smooth regions during the calibration phase for quantization boundaries.

### 3.1 PRELIMINARIES: QUANTIZATION

We first introduce model quantization (Jacob et al., 2018), which is employed to simulate quantization errors. Given a weight or activation tensor value  $v$  to be fake-quantized and a quantization bit-width  $b$ , the processing procedure can be formally expressed as:

$$\Delta = \frac{u - l}{2^b - 1}, \quad z = \text{clip}(\text{Round}(-\frac{l}{\Delta}), 0, 2^b - 1), \quad v_z = \text{clip}(\text{Round}(\frac{v}{\Delta}) + z, 0, 2^b - 1), \quad (1)$$

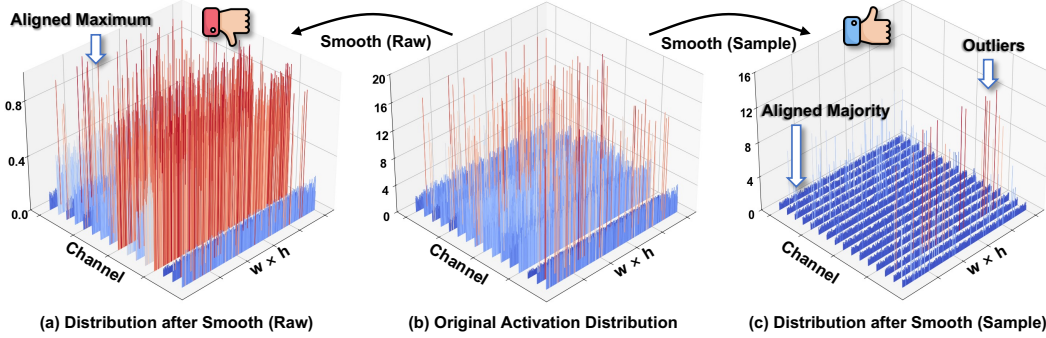


Figure 3: Activation distributions (Original, Smooth (Raw), Smooth (Sample)). (a) Original: ranges differ across channels; (b) Smooth (Raw): align maxima only; (c) Smooth (Sample): align the main body (excluding outliers), improving suitability for quantization.

where  $l$  and  $u$  denote the lower and upper quantization bounds,  $\Delta$  is the scaling factor,  $z$  is the zero-point offset, and  $v_z$  is the integer-coded value of  $v$ . The clipping function is defined as  $\text{clip}(v, l, u) = \max(\min(v, u), l)$ , while  $\text{Round}(\cdot)$  maps an input to its nearest integer. The corresponding dequantization process can be formulated as:

$$Q(v) = \Delta \times (v_z - z), \quad (2)$$

where  $Q(\cdot)$  denotes the operation of fake quantization. For a quantized convolutional layer, given the input activation  $\mathbf{X}$ , weight  $\mathbf{W}$ , and bias  $\mathbf{b}$ , the output  $\mathbf{Y}$  can be obtained through:

$$\mathbf{Y} = Q(\mathbf{X}) \cdot Q(\mathbf{W}) + \mathbf{b}. \quad (3)$$

Because  $\text{Round}(\cdot)$  is non-differentiable, following prior works (Qin et al., 2023; Li et al., 2024), the straight-through estimator (STE) is adopted to approximate its gradient:

$$\frac{\partial Q(v)}{\partial v} \approx \begin{cases} 1 & \text{if } v \in [l, u], \\ 0 & \text{otherwise.} \end{cases} \quad (4)$$

Moreover, SmoothQuant (Xiao et al., 2023) is widely adopted in quantization to address the challenge arising from the variation in maximum magnitudes across channels. It applies a per-channel scaling transformation to redistribute the quantization difficulty from activations to weights. Given an activation  $\mathbf{X}$  and a weight tensor  $\mathbf{W}$  for the  $j$ -th input channel, the smoothing factor  $s_j$  is defined as:

$$s_j = \max(|\mathbf{X}_j|)^\alpha / \max(|\mathbf{W}_j|)^{1-\alpha}, \quad \mathbf{s} = (s_1, s_2, \dots, s_n), \quad (5)$$

where  $\alpha$  is a balancing hyperparameter controlling the trade-off between activation and weight quantization,  $n$  denotes the number of input channels, and  $\mathbf{s}$  is the smoothing coefficient vector.

Despite these developments, existing quantization methods still lead to substantial performance degradation when applied to demoiréing models. Therefore, we propose the outlier-aware quantizer and the frequency-aware calibration strategy to enhance the performance of demoiréing.

### 3.2 OUTLIER-AWARE QUANTIZER

**Challenges.** Despite the progress in neural network quantization, existing methods still face critical limitations, particularly due to the presence of outliers. They can lead to two key problems: **quantization range expansion** and **inaccurate smoothing factor estimation**.

**Challenge I. Quantization range expansion.** Outliers enlarge the quantization range either within a single channel or across the entire tensor, thereby reducing information density and, as a result, further aggravating quantization error for normal values.

**Challenge II. Inaccurate smoothing factor estimation.** When the maximum absolute value, which is an outlier, is used to compute the smoothing factor, the maximum values across channels can be aligned. However, as shown in Fig. 3 (Smooth (Raw)), significant range disparities remain among the non-outlier values across channels due to the large difference between outliers and non-outliers.

Some existing post-training quantization methods (such as percentile (Li et al., 2019)) are specifically designed to address the problems caused by outliers. However, these methods could lead to some additional time overhead during the calibration stage. At the same time, because of their inflexible design, these methods may lack robustness in the face of outliers in different distributions.

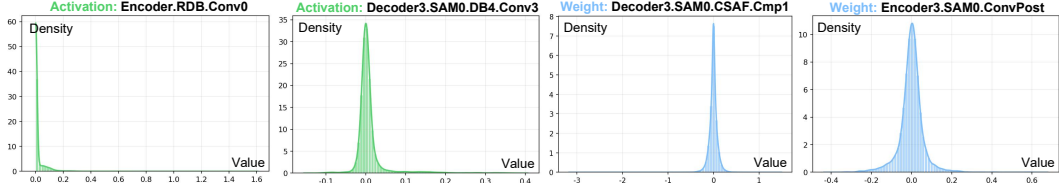


Figure 4: Visualization of **activation** and **weight** distributions from randomly selected layers in ESDNet (Yu et al., 2022). The distributions are approximately Gaussian or exponential.

**Sampling-Based Activation Quantizer.** To address the problems caused by outliers, we propose a random sampling-based method for estimating activation ranges. From Fig. 4, it can be observed that, most activations conform to either a Gaussian or an exponential distribution. Such distributions typically exhibit a small number of outliers that deviate from the normal range on one or both sides. More distribution visualizations are provided in the supplementary material to support this point.

To mitigate the impact of these outliers on quantization accuracy, we adopt a strategy of randomly sampling a small subset of activation values in a channel or tensor (Fig. 2a). Specifically,  $\text{Sample}_{\gamma}(\cdot)$  denotes a subset formed by randomly selecting a proportion  $\gamma$  of elements from the activations. This approach reduces the probability of selecting outliers, thereby alleviating the quantization error they introduce, while at the same time ensuring an accurate estimation of the distribution range of the majority of non-outlier values. We first use a small subset of the training dataset as a calibration dataset, and estimate the maximum magnitude of activations for each channel by randomly sampling:

$$M_j = \max(|\text{Sample}_{\gamma_1}(\mathbf{X}_j)|), \quad (6)$$

where  $\mathbf{X}_j$  is the  $j$ -th input channel of activation,  $M_j$  is the estimated maximum magnitude and,  $\gamma_1$  is the proportion of elements sampled from each activation channel. By restricting the estimation to a sampled subset, the proposed method effectively captures the typical distribution of activations while reducing the influence of outlier values. For the calculation of the maximum weight magnitude, we directly take the largest absolute value. The computation of the smoothing factor can be written as:

$$s_j = M_j^{\alpha} / \max(|\mathbf{W}_j|)^{1-\alpha}. \quad (7)$$

After being divided by the smooth scaling factor, the outliers still remain in the activation tensor. Therefore, we continue to estimate the outliers using a sampling approach with a proportion  $\gamma_2$ :

$$u_a = \max(\text{Sample}_{\gamma_2}(\mathbf{X} \otimes \mathbf{s})), \quad l_a = \min(\text{Sample}_{\gamma_2}(\mathbf{X} \otimes \mathbf{s})), \quad (8)$$

where  $l_a$ ,  $u_a$  denote the lower and upper bounds of the quantizer, respectively.  $\mathbf{X}$  represents the activation tensor and  $\mathbf{s}$  denotes the smoothing factor. By estimating quantization boundaries from the sampled subset, the quantization boundaries naturally discard extreme outliers, thereby focusing on the main distribution of activations. Visualizations in Fig. 3 reveal that Smooth (Sample) achieves better smoothing of non-outlier values (*i.e.*, the majority of the distribution).

Finally, the derived  $l_a$  and  $u_a$  are applied in Eq. (1) to perform activation quantization, forming the sampling-based activation quantizer. This quantizer is able to effectively mitigate the impact of outliers on the quantization accuracy, thereby improving model performance.

**Mixed-Precision Weight Quantizer.** As illustrated in Fig. 4, similar to the behavior observed in activation distributions, the weight distribution of the network exhibits an approximately Gaussian pattern. Therefore, the outliers of the weight mainly exist on the sides of the distribution. A straightforward way to handle these extreme values is to apply the same sampling-based estimation method proposed in activation quantization. However, unlike activations, weight tensors generally contain far fewer elements. Consequently, the direct truncation of extreme weight values would lead to a notable degradation in the performance of the quantized model.

To overcome this limitation, we propose preserving the outliers in FP16 precision. In this way, we improve the quantification accuracy of non-outliers. At the same time, by storing outliers separately, we avoid the potential performance degradation of the model that could arise from directly discarding them. The illustration is in Fig. 2a. By preserving a proportion  $\beta$  of outliers at both ends, we can calculate the corresponding lower and upper percentile thresholds:  $T_{\text{low}} = P_{\beta}(\mathbf{W})$  and  $T_{\text{high}} = P_{1-\beta}(\mathbf{W})$ . Here,  $P_{\beta}(\mathbf{W})$  denotes the  $\beta$ -th percentile of  $\mathbf{W}$ . The complete weight quantization process can then be expressed as follows:

$$\begin{aligned} \mathbf{W}_{\text{outlier}} &= \{w_i \in \mathbf{W} \mid w_i < T_{\text{low}} \text{ or } w_i > T_{\text{high}}\}, \\ \mathbf{W}_{\text{normal}} &= \mathbf{W} \setminus \mathbf{W}_{\text{outlier}}, \quad \hat{\mathbf{W}} = \mathbf{W}_{\text{outlier}} \cup Q(\mathbf{W}_{\text{normal}}), \end{aligned} \quad (9)$$

where  $\mathbf{W}_{\text{outlier}}$  and  $\mathbf{W}_{\text{normal}}$  denote the sets of outlier and non-outlier weights, respectively;  $\hat{\mathbf{W}}$  represents the final quantized weight. Experimental results indicate that  $\beta = 0.005$  is sufficient to achieve this balance. By introducing only a minimal increase in parameter size, this approach mitigates quantization errors caused by outliers in weights, while still preserving the overall accuracy.

**Conclusion.** The proposed outlier-aware quantizer effectively addresses the limitations posed by extreme activation and weight values. By employing random sampling for activation range estimation and selectively retaining a small fraction of weight outliers in higher precision, the method mitigates quantization errors without incurring substantial computational or storage costs. This dual strategy balances efficiency with accuracy, ensuring robust model performance under quantization.

### 3.3 FREQUENCY-AWARE CALIBRATION STRATEGY

Conventional quantization boundary optimization typically employs a combination of pixel-wise reconstruction loss and perceptual loss. Although this method can optimize the performance to some extent, the quantized model still exhibits significant performance degradation. In particular, quantization affects frequency components unevenly. For high-frequency structures such as edges and textures, the distortions are relatively minor due to their sharp RGB variations. However, in low- and mid-frequency regions with gradual intensity transitions, quantization severely reduces representational capacity, often manifesting as color banding. As illustrated in Fig. 5, the output of the quantized model exhibits pronounced banding artifacts in smooth areas.

To address the above problem, we propose a frequency-aware calibration strategy. This method optimizes the parameters of the quantizer by extracting the mid- and low-frequency components from both the model outputs and the ground truth, then optimizing the loss accordingly. Specifically, following previous work (Liu et al., 2025; Wang et al., 2024), we employ a dedicated convolution kernel  $\mathbf{k}$  to extract the mid- and low-frequency components. The kernel  $\mathbf{k}$  can be formally defined as:

$$\mathbf{k} = \begin{bmatrix} 1/16 & 1/8 & 1/16 \\ 1/8 & 1/4 & 1/8 \\ 1/16 & 1/8 & 1/16 \end{bmatrix}. \quad (10)$$

The frequency extraction process is an  $L$ -step iterative procedure based on kernel  $\mathbf{k}$ . Given a image  $\mathbf{I}$ , in the  $i$ -th step ( $i = 1, 2, \dots, L$ ), the extraction can be formalized as:

$$\mathbf{I}^i = E_{\mathbf{k}}^i(\mathbf{I}^{i-1}), \quad (11)$$

where  $\mathbf{I}^0 = \mathbf{I}$ ,  $\mathbf{I}^i$  is the outcome of the  $i$ -th step of extraction.  $E_{\mathbf{k}}^i$  denotes an operation where the input is convolved with the kernel  $\mathbf{k}$  and a dilation of  $2^i$ . The whole **frequency extraction** process can be written as a recursive function  $F(\cdot)$ , which is defined as follows:

$$F(\mathbf{I}, i) = \begin{cases} \mathbf{I}, & i = 0, \\ E_{\mathbf{k}}^i(F(\mathbf{I}, i-1)), & i \geq 1. \end{cases} \quad (12)$$

The outcome of the whole frequency extraction procedure is  $F(\mathbf{I}, L)$ , which serves as the basis for loss computation. As shown in Fig. 2b, during the phase of optimizing quantization boundaries, we extract the low- and mid-frequency components from the output image and ground truth, and employ a pixel-wise  $\mathcal{L}_1$  loss together with a feature-based perceptual loss  $\mathcal{L}_p$  as the optimizing objective. The perceptual loss  $\mathcal{L}_p$  is computed as the  $L_1$  distance between the VGG16 feature (Yu et al., 2022).

Specifically, given the output of the quantitative model  $\mathbf{I}'$  and the corresponding ground truth  $\hat{\mathbf{I}}$ , the extracted component of low and mid frequencies are defined as  $\mathbf{I}'_l = F(\mathbf{I}', L)$  and  $\hat{\mathbf{I}}_l = F(\hat{\mathbf{I}}, L)$ , respectively. Then, we compute the loss  $\mathcal{L}_{\text{total}}$  on the extracted frequencies as follows:

$$\mathcal{L}_{\text{total}} = \mathcal{L}_1(\mathbf{I}'_l, \hat{\mathbf{I}}_l) + \mathcal{L}_p(\mathbf{I}'_l, \hat{\mathbf{I}}_l). \quad (13)$$

To improve calibration efficiency, we only optimize the quantization boundaries of activations while keeping all other parameters fixed. Besides, we find that when  $L$  is small (e.g.,  $L = 1$ ), more high-frequency information is preserved, whereas a larger  $L$  (e.g.,  $L = 5$ ) focuses only on low frequencies. Since our goal is to focus on both low- and mid-frequency regions, we set  $L = 3$ . Experiments in Sec. 4.2 (Tab. 3b) further validate this choice.

In summary, by incorporating mid- and low-frequency components into quantization boundary training, the proposed frequency-aware calibration strategy effectively alleviates the uneven impact of quantization across frequency bands. As shown in Fig. 5 (Mid&Low-Freq), this strategy significantly reduces banding artifacts caused by low-bit quantization.

Table 1: Ablation study on sampling-based activation quantizer.

(a) Quantizer bound calculation.

(b) Smooth transformation.

Method	MinMax	Percentile	Sample	Method	Original	Smooth (Raw)	Smooth (Sample)
PSNR $\uparrow$	16.51	16.85	<b>17.61</b>	PSNR $\uparrow$	17.61	20.43	<b>20.52</b>
SSIM $\uparrow$	0.5255	0.6701	<b>0.6892</b>	SSIM $\uparrow$	0.6892	0.7408	<b>0.7538</b>
LPIPS $\downarrow$	0.6786	0.4639	<b>0.4552</b>	LPIPS $\downarrow$	0.4552	0.3363	<b>0.3247</b>

Table 2: Ablation study on mixed-precision weight quantizer.

(a) Outlier handling method.

(b) Outliers Proportion ( $\beta$ ).

Method	Baseline	Discard Outliers	Store Random	Store Outlier	# $\beta$	PSNR $\uparrow$	SSIM $\uparrow$	LPIPS $\downarrow$	Params (M)	Ops (G)
PSNR $\uparrow$	20.52	16.29	20.54	<b>20.92</b>	0.25%	20.88	0.7565	0.3180	0.7837	1.78
SSIM $\uparrow$	0.7538	0.6724	0.7542	<b>0.7570</b>	0.50%	20.92	0.7570	0.3171	0.7948	1.80
LPIPS $\downarrow$	0.3247	0.4103	0.3244	<b>0.3171</b>	1.00%	21.04	0.7578	0.3171	0.8171	1.85

## 4 EXPERIMENTS

### 4.1 EXPERIMENTAL SETTINGS

**Datasets and Metrics.** We conduct experiments on three moiré pattern removal datasets: UHDM (Yu et al., 2022), FHDMi (He et al., 2020), and LCDMoiré (Yuan et al., 2019). For each dataset, we randomly select 200 image pairs from the training dataset and crop them to construct a calibration dataset. After the calibration stage, we evaluate the results on the corresponding test dataset. For quantitative assessment, we adopt PSNR, SSIM (Wang et al., 2004), and LPIPS (Zhang et al., 2018).

**Implementation Details.** We adopt ESDNet (Yu et al., 2022) as the backbone and provide results under 3, 4, 6, and 8 bits. The quantization setup is denoted as  $WwAa$ , where  $w$  and  $a$  are the bit widths of weights and activations. For the sampling rate, we set  $\gamma_1 = \gamma_2 = 10^{-3}$ . For the smoothing factor, we use  $\alpha = 0.5$ . Both our method and the compared baselines apply static quantization, with per-channel quantization for weights and per-tensor quantization for activations. The baselines and our method are fairly evaluated, with more **details** provided in the supplementary materials.

**Calibration Settings.** During optimization, the quantization parameters are trained for 4 epochs using the Adam (Kingma & Ba, 2015) optimizer with  $\beta_1 = 0.9$  and  $\beta_2 = 0.999$ . The image pairs are randomly cropped into  $512 \times 512$ , and the batch size is 1. The initial learning rate is set to 0.001 and scheduled with cyclic cosine annealing (Loshchilov & Hutter, 2017).

### 4.2 ABLATION STUDY

We investigate the impact of the proposed outlier-aware quantizer (for activations and weights) and the frequency-aware calibration strategy. All experiments are conducted on the UHDM (Yu et al., 2022) dataset with 4-bit quantization (W4A4). The experiment settings follow Sec. 4.1 to ensure fairness. Results are presented in Tabs. 1, 2, and 3, as well as Fig. 5.

**Activation Quantizer.** We evaluate different strategies for calculating activation quantization bounds in Tab. 1a. The baseline is the min-max method (Jacob et al., 2018). We compare it with the percentile (Li et al., 2019) and our proposed sample-based method (as in Eq. 7). Compared with previous boundary selection, our sampling-based approach proves more effective.

Furthermore, we introduce a smooth transformation to adjust channels within the sample-based framework. As illustrated in Fig. 3, we compare two variants: the original definition and our sample-based smoothing. Results in Tab. 1b show that outlier removal via sampling enhances the effectiveness of the smoothing. In general, our sample-based activation quantizer leads to more robust quantization.

**Weight Quantizer.** We compare different strategies for handling weight outliers in Tab. 2a. We adopt the smooth (sample-based) result from Tab. 1b as the baseline. The results show that, compared with randomly storing some weights in FP16, explicitly preserving outliers in FP16 is more effective. Besides, consistent with the analysis in Sec. 3.2, discarding outliers leads to a performance drop.

We further evaluate the proportion of outliers ( $\beta$ ) in Tab. 2b. The Ops are computed under an input size of  $3 \times 224 \times 224$ . We find that setting the ratio  $\beta=0.5\%$  achieves a favorable trade-off between efficiency and performance. Therefore, we adopt this setting as the default in QuantDemoire.

Table 3: Ablation study on frequency-aware calibration strategy.

(a) Calibration strategy.

(b) Frequency extraction level.

Method	No Calibration	Original Image	High-Freq	Mid&Low-Freq	Level	1	3	5
PSNR $\uparrow$	20.92	20.95	20.62	<b>21.08</b>	PSNR $\uparrow$	20.96	<b>21.08</b>	21.05
SSIM $\uparrow$	0.7570	0.7604	0.7538	<b>0.7626</b>	SSIM $\uparrow$	0.7605	<b>0.7626</b>	0.7605
LPIPS $\downarrow$	0.3171	0.3088	0.3275	<b>0.3068</b>	LPIPS $\downarrow$	0.3092	<b>0.3068</b>	0.3071



Figure 5: Visualization of results under different calibration strategies. Original: training in the spatial domain suffers from banding artifacts under low-bit quantization. Mid&Low-Freq: our frequency-aware calibration strategy leverages mid- and low-frequency to mitigate banding.

Table 4: Quantitative comparison with state-of-the-art methods. The best and second-best results are colored red and blue. Our method outperforms on various datasets and metrics.

Method	Bit	UHDM			FHDMi			LCDMoiré		
		PSNR $\uparrow$	SSIM $\uparrow$	LPIPS $\downarrow$	PSNR $\uparrow$	SSIM $\uparrow$	LPIPS $\downarrow$	PSNR $\uparrow$	SSIM $\uparrow$	LPIPS $\downarrow$
ESDNet (Yu et al., 2022)	W32A32	22.12	0.7956	0.2551	24.50	0.8351	0.1354	44.83	0.9963	0.0097
MinMax (Jacob et al., 2018)	W8A8	21.50	0.7727	0.2596	20.30	0.7631	0.2600	37.92	0.9865	0.0236
Percentile (Li et al., 2019)	W8A8	19.38	0.7744	0.2784	19.73	0.7519	0.2734	30.11	0.9585	0.0281
2DQuant (Liu et al., 2024)	W8A8	21.20	0.7827	0.2749	20.57	0.7861	0.2034	<b>41.60</b>	<b>0.9923</b>	0.0214
SVDQuant (Li et al., 2024)	W8A8	<b>21.80</b>	<b>0.7907</b>	<b>0.2580</b>	<b>22.07</b>	<b>0.7966</b>	<b>0.1598</b>	41.18	0.9915	<b>0.0165</b>
QuantDemoire (ours)	W8A8	<b>22.00</b>	<b>0.7932</b>	<b>0.2555</b>	<b>22.23</b>	<b>0.8026</b>	<b>0.1591</b>	<b>42.16</b>	<b>0.9930</b>	<b>0.0126</b>
MinMax (Jacob et al., 2018)	W6A6	20.48	<b>0.7648</b>	<b>0.2828</b>	19.85	0.7362	0.3040	24.53	0.9337	0.1692
Percentile (Li et al., 2019)	W6A6	18.44	0.7562	0.2957	19.22	0.7353	0.2953	22.46	0.9342	<b>0.1074</b>
2DQuant (Liu et al., 2024)	W6A6	20.02	0.7595	0.2893	20.66	<b>0.7389</b>	<b>0.2558</b>	26.53	0.9366	0.2241
SVDQuant (Li et al., 2024)	W6A6	<b>20.86</b>	0.7602	0.3015	<b>20.91</b>	0.6883	0.3732	<b>32.10</b>	<b>0.9691</b>	0.1314
QuantDemoire (ours)	W6A6	<b>21.61</b>	<b>0.7874</b>	<b>0.2572</b>	<b>21.63</b>	<b>0.7861</b>	<b>0.1721</b>	<b>40.48</b>	<b>0.9910</b>	<b>0.0206</b>
MinMax (Jacob et al., 2018)	W4A4	16.51	0.5255	0.6786	16.01	0.4958	0.6686	15.14	0.7031	0.7500
Percentile (Li et al., 2019)	W4A4	16.85	<b>0.6701</b>	0.4639	<b>16.92</b>	<b>0.6424</b>	<b>0.4858</b>	14.95	<b>0.8290</b>	<b>0.5596</b>
2DQuant (Liu et al., 2024)	W4A4	<b>17.07</b>	0.6288	<b>0.5117</b>	14.80	0.3579	0.7107	15.11	0.6075	0.7561
SVDQuant (Li et al., 2024)	W4A4	14.68	0.5762	0.6559	12.43	0.2818	0.7961	<b>15.25</b>	0.7201	0.6687
QuantDemoire (ours)	W4A4	<b>21.08</b>	<b>0.7626</b>	<b>0.3068</b>	<b>20.28</b>	<b>0.6745</b>	<b>0.3369</b>	<b>31.28</b>	<b>0.9544</b>	<b>0.1793</b>
MinMax (Jacob et al., 2018)	W3A3	12.53	0.3802	0.8630	12.16	0.2903	0.8514	10.11	<b>0.6051</b>	<b>0.8376</b>
Percentile (Li et al., 2019)	W3A3	14.79	<b>0.5206</b>	<b>0.6869</b>	<b>14.33</b>	<b>0.4444</b>	<b>0.7496</b>	9.30	0.5242	1.0272
2DQuant (Liu et al., 2024)	W3A3	11.20	0.2465	0.8460	10.92	0.2879	0.8612	9.07	0.3026	1.0153
SVDQuant (Li et al., 2024)	W3A3	<b>14.83</b>	0.4547	0.7289	9.34	0.2127	0.8840	<b>10.17</b>	0.5658	0.9753
QuantDemoire (ours)	W3A3	<b>19.12</b>	<b>0.6839</b>	<b>0.4567</b>	<b>18.26</b>	<b>0.5722</b>	<b>0.4930</b>	<b>22.02</b>	<b>0.8558</b>	<b>0.4544</b>

**Calibration Strategy.** We conduct an ablation study on different calibration strategies for optimizing quantized parameters. We apply the outlier-aware quantizer as the baseline. Results in Tab. 3a show that focusing on mid- and low-frequency components yields better performance.

We also evaluate different levels of frequency extraction (Tab. 3b). The relatively high (level=1) or low (level=5) frequencies are not optimal. In contrast, level=3 achieves better performance, which aligns with our analysis. Besides, we visualize results under different calibration strategies in Fig. 5. Our calibration strategy alleviates banding artifacts caused by quantization.

#### 4.3 COMPARISON WITH STATE-OF-THE-ART METHODS

We utilize ESDNet (Yu et al., 2022) as the full-precision backbone and compare QuantDemoire with several advanced post-training quantization methods, including MinMax (Jacob et al., 2018), Percentile (Li et al., 2019), 2DQuant (Liu et al., 2024), and SVDQuant (Li et al., 2024).

**Quantitative Results.** Quantitative evaluations are summarized in Tab. 4. Across all datasets, bit-widths, and metrics, our approach consistently delivers superior performance. Notably, the improvements are more pronounced at lower bit-widths (*e.g.*, 4/3-bit). For example, under the 4-bit setting, our approach surpasses the latest method, SVDQuant (Li et al., 2024), by more than **6 dB** on the UHDM (Yu et al., 2022) dataset. Furthermore, our model retains performance close to the full-precision network under 8/6-bit settings, while the degradation at 3/4-bit is greatly reduced. More results and analyses (especially for SVDQuant) are provided in the supplementary material.



Figure 6: Visual comparison on UHDM (Yu et al., 2022), FHDMI (He et al., 2020), and LCD-Moiré (Yuan et al., 2019) datasets. Our QuantDemoire outperforms other quantization methods.

**Qualitative Results.** We present visual comparisons across 3-bit, 4-bit, and 6-bit settings on different datasets in Fig. 6. Existing quantization baselines tend to leave residual moiré artifacts or fail to reconstruct clean structures, especially on difficult samples and at lower precision. In contrast, our QuantDemoire effectively removes moiré patterns and restores fine image details. Meanwhile, our QuantDemoire maintains results that are very close to full precision, even at low bit-widths (e.g., 3-bit). This observation is consistent with the quantitative results in Tab. 4. More visual results on various datasets and bit settings are provided in the supplementary material.

**Compression Ratio.** We report the parameter (Params) and operation (Ops) compression ratios at 6/4/3-bit in Tab. 5. The Ops are measured with an input size of  $3 \times 224 \times 224$ . Compared with the full-precision (32-bit) model, our approach significantly reduces both model size and computational cost. At 4-bit, the compression rate exceeds 86.6%, while the performance drop is limited to 4.7% (PSNR). Moreover, compared with existing quantization methods, QuantDemoire demonstrates clear advantages. For instance, compared to 2DQuant, it achieves over a 4 dB gain with only a negligible increase in overhead. More results on compression ratios are provided in the supplementary material.

Table 5: Compression ratios of Params and Ops at 6/4/3-bit. Ops are measured with an input size of  $3 \times 224 \times 224$ .

Method	Bit (w/a)	Params (M) (↓Ratio)	Ops (G) (↓Ratio)	UHDM	
				PSNR ↑	SSIM ↑
ESDNet	32/32	5.93 (↓0%)	13.52 (↓0%)	22.12	0.7956
2DQuant	6/6	1.12 (↓81.14%)	2.54 (↓81.25%)	20.02	0.7595
SVDQuant	6/6	1.45 (↓75.53%)	4.60 (↓65.97%)	20.86	0.7602
QuantDemoire	6/6	1.16 (↓80.43%)	2.64 (↓80.49%)	21.61	0.7874
2DQuant	4/4	0.75 (↓87.38%)	1.69 (↓87.50%)	17.07	0.6288
SVDQuant	4/4	1.08 (↓81.78%)	3.76 (↓72.19%)	14.68	0.5762
QuantDemoire	4/4	0.79 (↓86.61%)	1.80 (↓86.68%)	21.08	0.7626
2DQuant	3/3	0.56 (↓90.51%)	1.27 (↓90.63%)	11.20	0.2465
SVDQuant	3/3	0.90 (↓84.89%)	3.34 (↓75.30%)	14.83	0.4547
QuantDemoire	3/3	0.61 (↓89.69%)	1.38 (↓89.78%)	19.12	0.6839

## 5 CONCLUSION

In this paper, we propose QuantDemoire, a post-training quantization method tailored for image demoiréing. Our design is developed from two perspectives: the quantizer and the calibration strategy. We first introduce the outlier-aware quantizer to reduce quantization errors caused by outliers. We Besides, we develop a frequency-aware calibration strategy emphasizing mid- and low-frequency components to mitigate banding artifacts caused by low-bit quantization. Comprehensive experiments verify that our method effectively reduces overhead compared with the full-precision model. Meanwhile, QuantDemoire outperforms current advanced quantization methods.

## REFERENCES

Mengzhao Chen, Wenqi Shao, Peng Xu, Jiahao Wang, Peng Gao, Kaipeng Zhang, Yu Qiao, and Ping Luo. Efficientqat: Efficient quantization-aware training for large language models. *arXiv preprint arXiv:2407.11062*, 2024.

Xi Cheng, Zhenyong Fu, and Jian Yang. Multi-scale dynamic feature encoding network for image demoiréing. In *ICCVW*, 2019.

Tim Dettmers, Mike Lewis, Younes Belkada, and Luke Zettlemoyer. Gpt3. int8 (): 8-bit matrix multiplication for transformers at scale. In *NeurIPS*, 2022.

Steven K Esser, Jeffrey L McKinstry, Deepika Bablani, Rathinakumar Appuswamy, and Dharmendra S Modha. Learned step size quantization. *arXiv preprint arXiv:1902.08153*, 2019.

Bin He, Ce Wang, Boxin Shi, and Ling-Yu Duan. Mop moire patterns using mopnet. In *ICCV*, 2019.

Bin He, Ce Wang, Boxin Shi, and Ling-Yu Duan. Fhde2net: Full high definition demoiréing network. In *ECCV*, 2020.

Itay Hubara, Yury Nahshan, Yair Hanani, Ron Banner, and Daniel Soudry. Accurate post training quantization with small calibration sets. In *ICML*, 2021.

Benoit Jacob, Skirmantas Kligys, Bo Chen, Menglong Zhu, Matthew Tang, Andrew Howard, Hartwig Adam, and Dmitry Kalenichenko. Quantization and training of neural networks for efficient integer-arithmetic-only inference. In *CVPR*, 2018.

Diederik Kingma and Jimmy Ba. Adam: A method for stochastic optimization. In *ICLR*, 2015.

Muyang Li, Yujun Lin, Zhekai Zhang, Tianle Cai, Xiuyu Li, Junxian Guo, Enze Xie, Chenlin Meng, Jun-Yan Zhu, and Song Han. Svdquant: Absorbing outliers by low-rank components for 4-bit diffusion models. *arXiv preprint arXiv:2411.05007*, 2024.

Rundong Li, Yan Wang, Feng Liang, Hongwei Qin, Junjie Yan, and Rui Fan. Fully quantized network for object detection. In *CVPR*, 2019.

Xiuyu Li, Yijiang Liu, Long Lian, Huanrui Yang, Zhen Dong, Daniel Kang, Shanghang Zhang, and Kurt Keutzer. Q-diffusion: Quantizing diffusion models. In *ICCV*, 2023.

Fanglei Liu, Jingyu Yang, and Huanjing Yue. Moiré pattern removal from texture images via low-rank and sparse matrix decomposition. In *VCIP*, 2015.

Kai Liu, Haotong Qin, Yong Guo, Xin Yuan, Linghe Kong, Guihai Chen, and Yulun Zhang. 2dquant: Low-bit post-training quantization for image super-resolution. In *NeurIPS*, 2024.

Xiaoyang Liu, Bolin Qiu, Jiezhang Cao, Zheng Chen, Yulun Zhang, and Xiaokang Yang. Freqformer: Image-demoiréing transformer via efficient frequency decomposition. *arXiv preprint arXiv:2505.19120*, 2025.

Zhenhua Liu, Yunhe Wang, Kai Han, Wei Zhang, Siwei Ma, and Wen Gao. Post-training quantization for vision transformer. In *NeurIPS*, 2021.

Ilya Loshchilov and Frank Hutter. Sgdr: Stochastic gradient descent with warm restarts. In *ICLR*, 2017.

Markus Nagel, Marios Fournarakis, Rana Ali Amjad, Yelysei Bondarenko, Mart Van Baalen, and Tijmen Blankevoort. A white paper on neural network quantization. *arXiv preprint arXiv:2106.08295*, 2021.

Haotong Qin, Yulun Zhang, Yifu Ding, Xianglong Liu, Martin Danelljan, Fisher Yu, et al. Quantsr: accurate low-bit quantization for efficient image super-resolution. In *NeurIPS*, 2023.

Yuzhang Shang, Zhihang Yuan, Bin Xie, Bingzhe Wu, and Yan Yan. Post-training quantization on diffusion models. In *CVPR*, 2023.

---

Denis N Sidorov and Anil Christopher Kokaram. Suppression of moiré patterns via spectral analysis. In *VCIP*, 2002.

Ce Wang, Bin He, Shengsen Wu, Renjie Wan, Boxin Shi, and Ling-Yu Duan. Coarse-to-fine disentangling demoiréing framework for recaptured screen images. *TPAMI*, 2023.

Jianyi Wang, Zongsheng Yue, Shangchen Zhou, Kelvin CK Chan, and Chen Change Loy. Exploiting diffusion prior for real-world image super-resolution. *IJCV*, 2024.

Zhou Wang, Alan C Bovik, Hamid R Sheikh, and Eero P Simoncelli. Image quality assessment: from error visibility to structural similarity. *TIP*, 2004.

Guangxuan Xiao, Ji Lin, Mickael Seznec, Hao Wu, Julien Demouth, and Song Han. Smoothquant: Accurate and efficient post-training quantization for large language models. In *ICML*, 2023.

Zeyu Xiao, Zhihe Lu, and Xinchao Wang. P-bic: Ultra-high-definition image moiré patterns removal via patch bilateral compensation. In *ACM MM*, 2024.

Shuning Xu, Binbin Song, Xiangyu Chen, and Jiantao Zhou. Image demoiréing in raw and srgb domains. *arXiv preprint arXiv:2312.09063*, 2023.

Xin Yu, Peng Dai, Wenbo Li, Lan Ma, Jiajun Shen, Jia Li, and Xiaojuan Qi. Towards efficient and scale-robust ultra-high-definition image demoiréing. In *ECCV*, 2022.

Shanxin Yuan, Radu Timofte, Gregory Slabaugh, Aleš Leonardis, Bolun Zheng, Xin Ye, Xiang Tian, Yaowu Chen, Xi Cheng, Zhenyong Fu, et al. Aim 2019 challenge on image demoiréing: Methods and results. In *ICCVW*, 2019.

Richard Zhang, Phillip Isola, Alexei A Efros, Eli Shechtman, and Oliver Wang. The unreasonable effectiveness of deep features as a perceptual metric. In *CVPR*, 2018.

Bolun Zheng, Shanxin Yuan, Gregory Slabaugh, and Ales Leonardis. Image demoiréing with learnable bandpass filters. In *CVPR*, 2020.